



Disulfide-containing polymer delivery of C527 and a Platinum(IV) prodrug selectively inhibited protein ubiquitination and tumor growth on cisplatin resistant and patient-derived liver cancer models



Kun Shang^a, Lingpu Zhang^b, Yingjie Yu^b, Haihua Xiao^{c,*}, Yajuan Gao^{d,e}, Liu Yang^{d,f}, Jia Huang^{g,**}, Haiqin Song^{h,***}, Hongbin Han^{d,i,****}

^a Institute of Medical Technology, Peking University Health Science Center, Beijing, 100191, China

^b State Key Laboratory of Organic-Inorganic Composites, Beijing University of Chemical Technology, Beijing, 100029, China

^c Beijing National Laboratory for Molecular Science, State Key Laboratory of Polymer Physics and Chemistry, Institute of Chemistry, Chinese Academy of Science, Beijing, 100190, China

^d Department of Radiology, Peking University Third Hospital, Beijing, 100191, China

^e NMPA key Laboratory for Evaluation of Medical Imaging Equipment and Technique, Beijing, 100191, China

^f Beijing Key Laboratory of Magnetic Resonance Imaging Devices and Technology, Peking University Third Hospital, Beijing, 100191, China

^g Department of Hepatobiliary Surgery, China-Japan Friendship Hospital, Beijing, 100029, China

^h Department of General Surgery, Ruijin Hospital, Shanghai Jiaotong University, School of Medicine, Shanghai, 20023, China

ⁱ Peking University Shenzhen Graduate School, Shenzhen, 518055, China

ARTICLE INFO

Keywords:

Ubiquitination

Resistance of platinum drugs

PDX model

ABSTRACT

USP1 (Ubiquitin-specific protease 1) is closely related to the prognosis of patients with liver cancer and plays an important role in DNA damage repair. C527 is a selective USP1 inhibitor (USP1i), which can regulate the protein ubiquitination to effectively inhibit the proliferation of cancer cells. However, its clinical application is hindered due to the poor water solubility and lack of tumor targeting. Moreover, the efficacy of single use of USP1i is still limited. Herein, a glutathione (GSH) sensitive amphiphilic polymer (poly (2-HD-co-HPMDA)-mPEG, PHHM) with disulfide bonds in the main chain was designed to encapsulate the USP1i as well as platinum (IV) prodrug (Pt (IV)-C12), resulting in the formation of composite nanoparticles, i.e., NP-Pt-USP1i. NP-Pt-USP1i can inhibit the DNA damage repair by targeting USP1 by the encapsulated USP1i, which ultimately increases the sensitivity of tumor cells to cisplatin and enhances the anti-cancer efficacy of cisplatin. Finally, an intraperitoneal tumor mice model and a patient-derived xenograft (PDX) of liver cancer mice model were established to prove that NP-Pt-USP1i could effectively inhibit the tumor growth. This work further validated the possibility of therapeutically target USP1 by USP1i in combination with DNA damaging alkylating agents, which could become a promising cancer treatment modality in the future.

1. Introduction

Protein ubiquitination is the specific modification of some proteins in cells after translation, which becomes an indispensable regulation process of cell function [1–3]. Studies have shown that ubiquitination processes of many proteins [4], including gene expression [5], cell cycle progression [6], apoptosis [7], and DNA repair [8], can promote the

development of tumor [9,10]. The ubiquitination of a certain protein is therefore controlled in a concerted manner by ubiquitin E3 ligase and de-ubiquitinases (DUBs) in which the ubiquitination is mainly mediated by the DUBs [11]. The ubiquitination can result in the decomposition and release of ubiquitin from the substrate proteins, thereby avoiding the degradation of some certain proteins [12,13].

Ubiquitin-specific protease 1 (USP1) is one of the most typical DUB

* Corresponding author.

** Corresponding author.

*** Corresponding author.

**** Corresponding author. Department of Radiology, Peking University Third Hospital, 49 North Garden Road, Haidian District, Beijing, 100191, China.

E-mail addresses: hxiao@iccas.ac.cn (H. Xiao), huangjia@zryhy.com.cn (J. Huang), shq604shq@163.com (H. Song), hanhongbin@bjmu.edu.cn (H. Han).

<https://doi.org/10.1016/j.mtbio.2023.100548>

Received 30 November 2022; Received in revised form 7 January 2023; Accepted 11 January 2023

Available online 13 January 2023

2590-0064/© 2023 Published by Elsevier Ltd. This is an open access article under the CC BY-NC-ND license (<http://creativecommons.org/licenses/by-nc-nd/4.0/>).

proteins [10]. Studies have indicated that USP1 could play an important role in DNA damage responses [14,15]. USP1 regulates DNA damage responses by de-ubiquitination of certain proteins in Fanconi Anemia (FA) and Translesion Synthesis (TLS) pathways [8,16], leading to drug resistance, cancer recurrence and metastasis [17]. In addition, USP1 can stabilize DNA binding inhibitor 1 (ID1) and promote cancer cell proliferation [18]. Therefore, USP1 becomes a new target for cancer therapy. For this specific reason, a series of USP1 inhibitor (USP1i, including C527 and ML-323, etc.) have been developed to be a class of targeted drugs with potential therapeutic effect that can regulate cancer cell ubiquitination [14,19]. However, studies have shown that the small molecule based drugs, both C527 and ML-323 in single use, did not show good anti-tumor ability in clinic [19]. Further studies indicated that these compounds can only show strong anti-tumor activity against tumors with homologous recombination defect (HRD) mutations. What's more, such small molecule based drugs of USP1i is generally poorly water-soluble, resulting in limited clinical applications.

Fanconi anemia (FA) and DNA translesion synthesis (TLS) pathways were the first DNA damage tolerance and repair pathways found to be regulated by reversible ubiquitination. Platinum anticancer drugs, such as cisplatin, oxaliplatin, and carboplatin, are the first-line anticancer alkylating agents in clinic practice [20,21]. These drugs can cause DNA damage and induce cell apoptosis by cross-linking with DNAs in cancer cells [22,23]. Unfortunately, the DNA repair machinery is powerful in cancer cells, resulting in resistance to platinum drugs [24,25]. DNA damage response pathways, particularly TLS and ICL repair, may have contributed to this resistance. Therefore, inhibition of DNA damage response pathways (TLS and FA) by targeting USP1 could improve the sensitivity of tumor cells to cisplatin [26,27].

Herein, a tumor microenvironment sensitive amphiphilic polymer with disulfide bonds in the polymer main chain was designed to encapsulate a selective USP1i (C527) together with a hydrophobic platinum (IV) pro-drug (Pt (IV)-C12) with aliphatic fat acid chains in the axial positions, resulting in a composite nanoparticle (NP-Pt-USP1i). NP-Pt-USP1i was supposed to cause DNA damage by released platinum drugs, i.e., cisplatin. Moreover, NP-Pt-USP1i could target USP1 by encapsulated C527 to inhibit the DNA damage repair pathway, so as to improve the sensitivity of tumor cells to cisplatin and therefore increase the efficacy of platinum drugs. What is more, the drug carriers can be degraded triggered by intracellular overexpressed glutathione (GSH), resulting in the dissociation of NP-Pt-USP1i. In this way, the encapsulated Pt (IV)-C12 can be reduced to release cisplatin *via* chemical reduction of platinum (IV) and the encapsulated USP1i can be released directly. On the one hand, cisplatin can further cross link with intracellular DNAs, resulting in DNA damage and cell apoptosis. On the other hand, USP1i can promote the ubiquitination of ID1 and FANCD2 proteins, reduce the homologous recombination (HR) repair, and finally enhance cisplatin activity. Subsequently, an intraperitoneal cisplatin resistant tumor model of standard liver cancer cells (7404DDP-LUC) and a patient derived liver cancer (PDX) animal model were established for drug screen *in vivo*. Whether NP-Pt-USP1i can effectively and selectively inhibit the cell ubiquitination, tumor growth, and cisplatin resistance depending on the above models was extensively studied. This work verified the possibility of using USP1 as a therapeutic target, which can be widely applied to other types of cancer to improve efficacy of platinum based chemotherapy and provide guidance for efficient cancer therapy.

2. Results and discussion

2.1. Inhibition of protein ubiquitination enhances cisplatin anticancer activity

In order to explore the role of USP1 in DNA damage response in liver cancer patients, the difference of USP1, FANCD2, and BRCA1 gene expression between liver cancer patients and healthy people was analyzed by the Cancer Genome Atlas (TCGA). The results showed that

the expression of the above genes in liver cancer patients was higher than that in healthy people (Fig. S1). Next, the correlation between the gene expression of USP1, FANCD2, and BRCA1 and the survival rate of patients was further studied by TCGA. The results by Gene Expression Profiling Interactive Analysis (GEPiA) clearly showed that patients with low expression of USP1, FANCD2, and BRCA1 genes could have a longer survival time (Fig. 1C, Fig. S2).

In order to further explore the correlation between USP1 and homologous recombination repair related genes (FANCD2 and BRCA1), the correlation regression analysis was conducted. The results showed that the expression of USP1 was positively correlated with the expression of FANCD2 and BRCA1 (Fig. 1D), and the correlation coefficients were $R = 0.63$ and $R = 0.72$, respectively. In conclusion, USP1 is likely to play an important role in the DNA damage response pathway, thereby becoming a promising therapeutic target for liver cancer.

The above bioinformatics analysis indicates that the expression of USP1 is negatively correlated with therapeutic effect in liver cancer patients in clinic, indicating the use of USP1i such as C527 to inhibit the USP1 expression is possible to inhibit DNA repair, resulting in increasing DNA damage caused by DNA alkylating agents such as cisplatin, finally enhancing the anti-tumor effect. In order to explore this, cisplatin resistant cell line, namely, BEL-7404DDP (liver cancer) was chosen for the subsequent study. BEL-7404DDP cells were then treated with cisplatin, C527, and combination of cisplatin and C527. The cytotoxicity of the above drugs and drug combinations were studied by an MTT test. The results showed that the combination of cisplatin and C527 showed obvious synergistic anti-tumor effect (combination index (CI) < 1) (Fig. S3). The above results indicated that cisplatin and the USP1i of C527 had a promising prospect for combination therapy. Inhibiting USP1 *via* USP1i has therefore become an effective new strategy to enhance the anti-tumor effect of platinum drugs.

2.2. Synthesis and characterization of PHHM and Pt (IV)-C12

C527 is an effective USP1i, but its poor water solubility and insolubility limit its great application. In order to deliver C527 for intracellular release, a GSH sensitive polymer (poly (2-HD-co-HPMDA)-mPEG, PHHM) with disulfide bonds in the polymer main chain was synthesized, and Pt (IV)-C12 was also synthesized (Scheme S1, Figs. S4 and S5) [22].

2.3. Preparation and characterization of nanoparticles

To prepare nanoparticles with Pt (IV)-C12 and C527, PHHM was adopted to firstly co-assemble with Pt (IV)-C12 into NP-Pt *via* a nanoprecipitation method. In the same way, Pt (IV)-C12 and C527 were co-encapsulated with PHHM to nanoparticles (NP-Pt-USP1i).

To study the physicochemical properties of the above nanoparticles, transmission electron microscopy (TEM) was used. The results showed that NP-Pt-USP1i was a uniform spherical nanoparticle with a diameter of ca. 120 nm (Fig. 2A). Further dynamic light scattering (DLS) characterization indicated that the average particle size of NP-Pt was ca. 103.8 nm (Fig. S6), while that of NP-Pt-USP1i was about 124.2 nm (Fig. 2B). Besides, the zeta potentials of NP-Pt and NP-Pt-USP1i were -6.81 and -19.0 mV, respectively (Fig. 2C), and the polydispersity indexes (PDI) were 0.187 and 0.078, respectively, indicating the above two nanoparticles were well dispersed in aqueous solutions (Fig. 2D). Since there are disulfide bonds in the polymer backbone of PHHM, it can be possibly activated by GSH overexpressed in cancer cells, resulting in polymer carrier degradation, nanoparticle dissociation, and drug release.

To explore this process, NP-Pt-USP1i was treated with 10 mM GSH for 24 h, and we found that the particle size of NP-Pt-USP1i changed from a unimodal curve to a clearly bimodal curve by DLS. Specifically, the peak at 124.2 nm changed to 260 nm (peak 1) and 16.31 nm (peak 2) (Fig. 2E), indicating that NP-Pt-USP1i might be dissociated triggered by GSH, where the peaks with large particle sizes may be for the polymer aggregates with poor solubility, and the peaks with small particle sizes may be

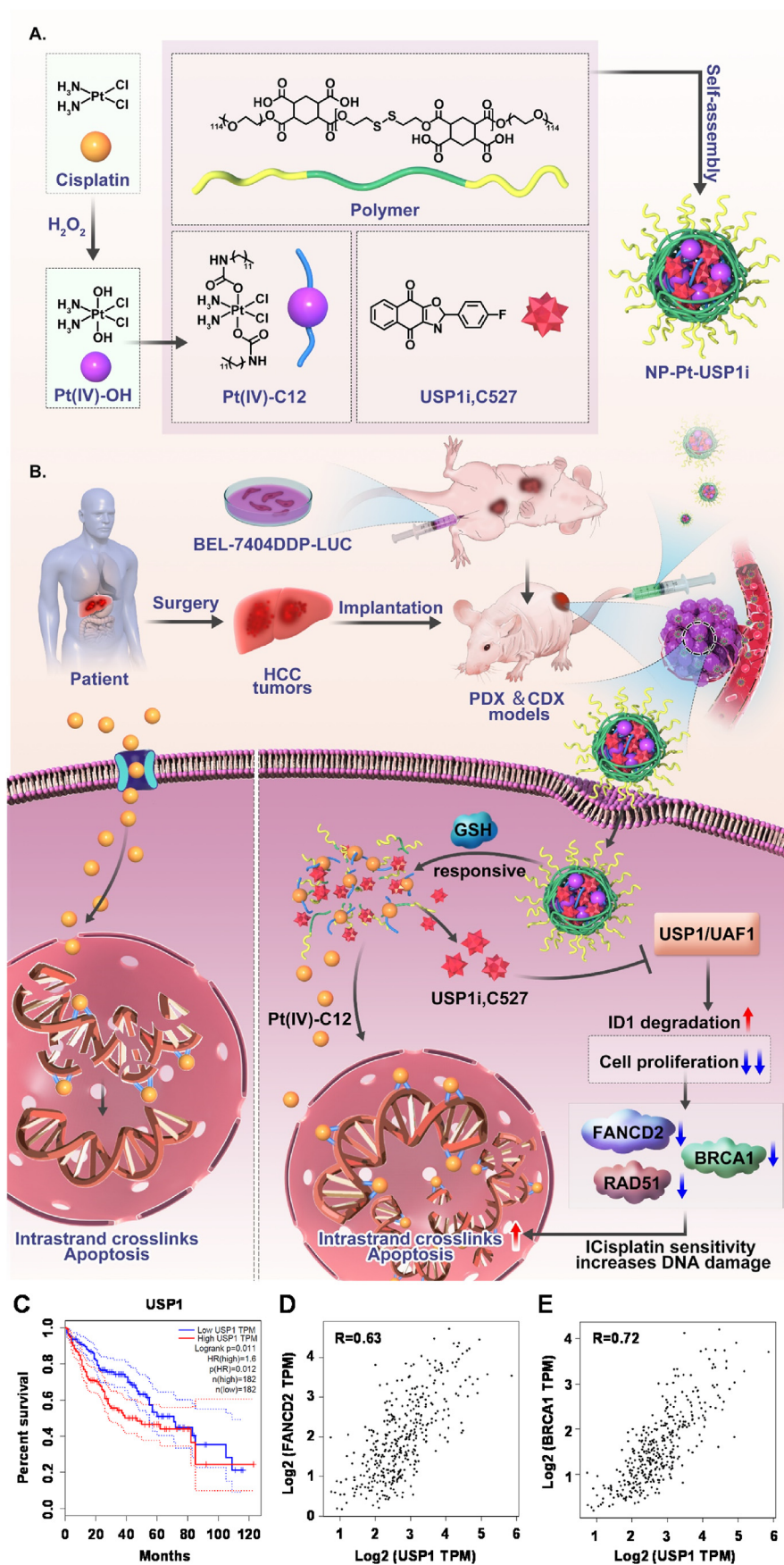


Fig. 1. USP1i (C527) sensitizes tumor cells to cisplatin via inhibition of USP1 which correlates with the treatment outcome of patients. A) Synthesis of Pt(IV)-C12, and preparation of NP-Pt-USP1i. B) The schematic illustration of NP-Pt-USP1i-enhanced chemotherapy. C) Kaplan-Meier analysis of overall survival probability in LIHC patients. Data were retrieved from TCGA datasets (<http://gepia.cancer-pku.cn/>). The patients were stratified according to high (n = 182) versus low (n = 182) expression of USP1 within their tumors. D) Correlation analysis (Pearson) of USP1 gene and FANCD2 gene in LIHC patients (n = 369). R² = 0.63. Data were retrieved from TCGA datasets (<http://gepia.cancer-pku.cn/>). E) Correlation analysis (Pearson) of USP1 gene and BRCA1 gene in LIHC patients (n = 369). R² = 0.72. Data were retrieved from TCGA datasets (<http://gepia.cancer-pku.cn/>).

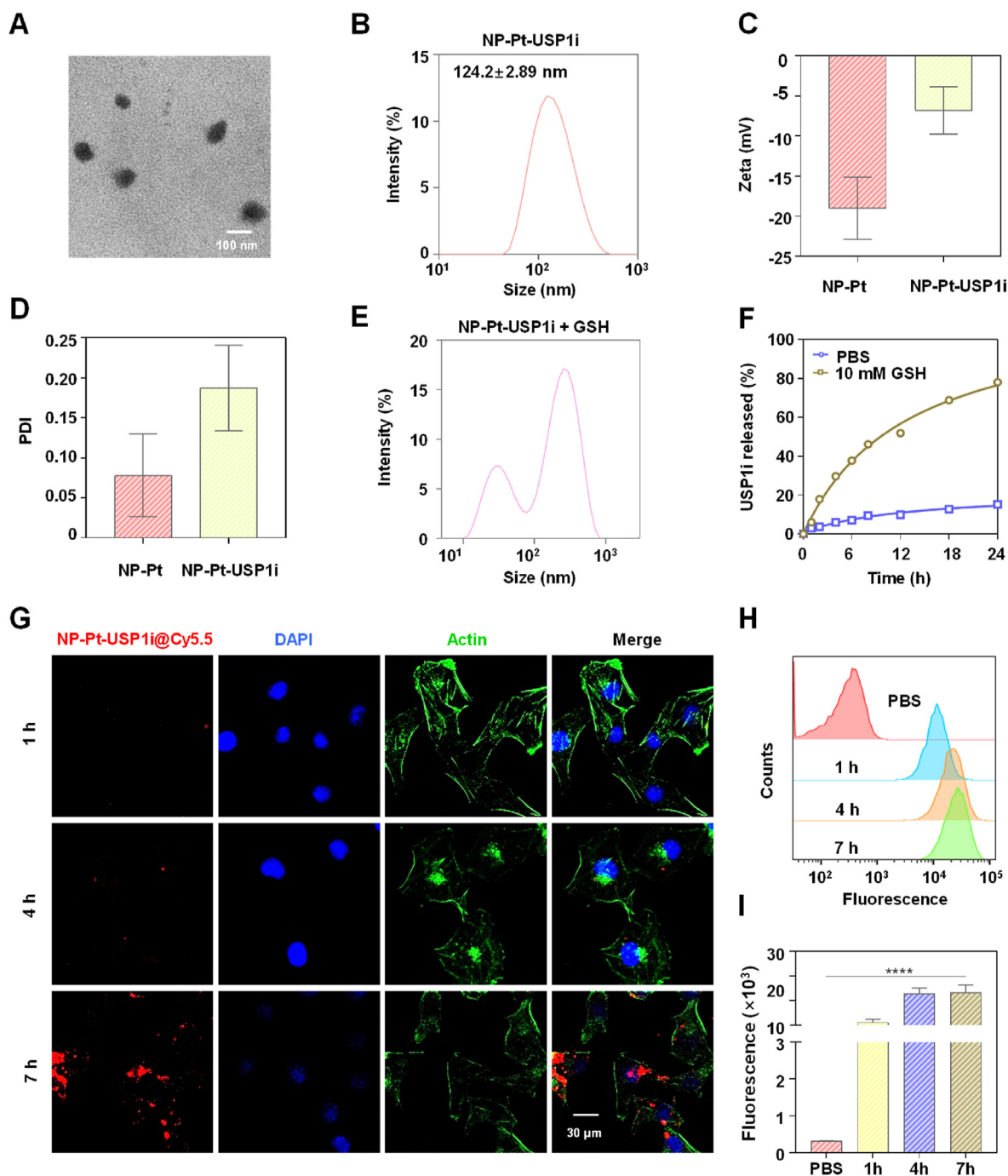


Fig. 2. Preparation, characterization and the intracellular uptake of NP-Pt-USP1i. A) Representative transmission electron microscopy (TEM) images of NP-Pt-USP1i. Scale bar = 100 nm. B) Particle size of NP-Pt-USP1i by DLS. C) Zeta potentials of NP-Pt and NP-Pt-USP1i by DLS. D) PDI of NP-Pt and NP-Pt-USP1i by DLS. E) The particle size of NP-Pt-USP1i after 24 h of exposure to 10 mM GSH. F) Cumulative C527 released from NP-Pt-USP1i by high performance liquid chromatography (HPLC) after 10 mM GSH treatment at different time points. G) The uptake of NP-Pt-USP1i@Cy5.5 by BEL-7404DPP cells by confocal laser microscopy after treatment for 1 h, 4 h and 7 h, respectively. The blue fluorescence comes from DAPI in the stained cell nucleus, and the red fluorescence comes from NP-Pt-USP1i@Cy5.5. The green fluorescence comes from the cytoskeleton stained with Alexa-488. Scale bar = 30 μ m. H) Flow cytometry was used to detect the uptake of NP-Pt-USP1i@Cy5.5 by BEL-7404DPP cells at 0 h, 1 h, 4 h and 7 h. I) Semi-quantitative analysis of the uptake. Data represent mean \pm standard deviation (SD) from n independent experiments ($n = 3$). **** $p < 0.0001$ (ordinary one-way ANOVA).

aggregates of polymer fragments with high solubility. Subsequently, the cumulative release of C527 from NP-Pt-USP1i was studied by high performance liquid chromatography (HPLC). Results showed that the release of C527 reached 80% after NP-Pt-USP1i was treated with 10 mM GSH for 24 h, fully indicating that NP-Pt-USP1i displayed a reduction-sensitive drug release behavior (Fig. 2F).

2.4. Uptake of NP-Pt-USP1i in vitro

The intracellular uptake of NP-Pt-USP1i by cancer cells is the key step for exerting anti-cancer effect. Therefore, in order to evaluate the ability of cancer cells to internalize NP-Pt-USP1i, a fluorescent dye of Cy5.5 was used to label the nanoparticles of NP-Pt-USP1i (NP-Pt-USP1i@Cy5.5). First, confocal laser microscopy (CLSM) was used to visualize the uptake

of NP-Pt-USP1i@Cy5.5 by cancer cells. The results showed that the red fluorescence in cells (mainly from the nanoparticles) was mainly distributed in the cells, and the red fluorescence intensity increased significantly with increasing drug incubation time, indicating that the uptake of NP-Pt-USP1i@Cy5.5 by cells was time-dependent (Fig. 2G). Subsequently, flow cytometry (FCM) was used to study the uptake of NP-Pt-USP1i@Cy5.5 by cancer cells. A semi-quantitative study was conducted on the uptake of nanoparticles (Fig. 2H). The results showed that the intensity of intracellular fluorescence for the cells treated with NP-Pt-USP1i@Cy5.5 increased with longer incubation time as well. Specifically, the fluorescence intensity at 7 h in the cancer cells was 2.5 times that of the fluorescence intensity at 1 h (Fig. 2I). The above results indicated NP-Pt-USP1i could be efficiently internalized by cancer cells in a time dependent manner.

To further determine whether NP-Pt-USP1i could promote the uptake of cisplatin by cancer cells, the platinum in BEL-7404 cells treated with cisplatin, NP-Pt, and NP-Pt-USP1i was quantified by ICP-MS [28]. After incubation for 24 h, the Pt uptake in BEL-7404 cells treated with NP-Pt and NP-Pt-USP1i reached about 198 ng Pt/million cells and 196 ng Pt/million cells, respectively, approximately 2.6 times the amount of that in cells treated with cisplatin (about 76.62 ng Pt/million cells) (Fig. S7A). Cisplatin is known to cause apoptosis of cancer cells by forming DNA cross-links. To this end, the difference in the formation of Pt-DNA adducts was evaluated in BEL-7404 cells treated by cisplatin, NP-Pt, and NP-Pt-USP1i. The results showed that the Pt-DNA adducts in BEL-7404 cells treated with cisplatin reached about 169.1 ng Pt/ 10^6 DNA, whereas these were 315.0 ng Pt/ 10^6 DNA and 527.0 ng Pt/ 10^6 DNA in BEL-7404 cells treated with NP-Pt and NP-Pt-USP1i, respectively (Fig. S7B). In summary, NP-Pt-USP1i can increase cellular uptake of platinum and the Pt-DNA adducts formation.

2.5. Antitumor activity of NP-Pt-USP1i *in vitro*

NP-Pt-USP1i can induce protein ubiquitination, and damage to biological macromolecules including DNAs, proteins, and lipids, etc., resulting in toxicity to the cancer cells. Therefore, the cytotoxicity of NP-Pt-USP1i was first evaluated on cisplatin sensitive and cisplatin resistant liver cancer cells (BEL-7404, BEL-7404DPP) and lung cancer (A549, A549DPP) cells via an MTT assay.

The results showed that cisplatin had a modest anti-tumor effect, while NP-Pt displayed better anti-tumor activity than cisplatin, and NP-Pt-USP1i had the strongest anti-tumor effect of all (Fig. 3A). Specifically, in BEL-7404 cells, the IC_{50} of NP-Pt-USP1i, NP-Pt and cisplatin are 2.3 μ M, 7.6 μ M, and > 40 μ M, respectively (Fig. 3B). The results indicated that NP-Pt-USP1i had higher anticancer activity than both NP-Pt and cisplatin. In BEL-7404DPP cells, the anti-tumor activity of NP-Pt-USP1i was also found to be significantly higher than that of other drugs. Among them, IC_{50} of NP-Pt-USP1i was 16.4 μ M. However, the IC_{50} of NP-Pt is > 40 μ M (Fig. 3B). The above results showed that even in cisplatin resistant liver cancer cells, NP-Pt-USP1i could effectively kill them, while cisplatin and NP-Pt were ineffective. In addition, in A549DDP cells, the IC_{50} of NP-Pt-USP1i was 10.1 μ M, while the IC_{50} values of cisplatin and NP-Pt were greater than 40 μ M (Fig. 3B). This also indicated that in cisplatin resistant A549DDP cells, NP-Pt-USP1i still had better anti-tumor activity.

Next, the apoptosis of BEL-7404DPP cells treated with different drugs was studied by an Annexin V-FITC and propidium iodide (PI) double staining assay. The results showed that the apoptosis rate of BEL-7404DPP cells treated with NP-Pt-USP1i ($16.26 \pm 1.8\%$) was 5.7 times that of cells treated with PBS ($2.85 \pm 0.99\%$) (Fig. 3C and D). Subsequently, the effect of NP-Pt-USP1i on the clonony formation of BEL-7404DPP cells was further studied. To make it simpler, the BEL-7404DPP cells were treated with various drugs, which were then cultured for two weeks for further observation on the cell colonies via a crystal violet assay. The results showed that the number of cell colonies

formed by cells treated with cisplatin was significantly higher than those formed in cells treated with NP-Pt-USP1i (Fig. 3E and F). The above results clearly showed that NP-Pt-USP1i could significantly inhibit the BEL-7404DPP growth *in vitro*. Finally, in order to explore the anti-tumor effect of NP-Pt-USP1i *in vitro*, BEL-7404 cells were adopted to culture a 3D tumor spheroid. In this way, the anti-tumor activity of NP-Pt-USP1i was studied by a live and dead staining assay of the 3D tumor spheroid (Fig. 3G). The results showed that the number of dead cells (red fluorescence signal) in the 3D tumor spheroid treated with NP-Pt-USP1i was significantly more than those in the 3D tumor spheroid treated with other drugs (Fig. 3H). To sum up, NP-Pt-USP1i showed more efficient tumor cell killing ability both on 2D cells and 3D tumor spheroid *in vitro*.

2.6. NP-Pt-USP1i can increase DNA damage of tumor cells *in vitro*

After NP-Pt-USP1i enters the cells, they can be triggered by the overexpressed GSH in the cancer cells, resulting in the breakdown of the disulfide bonds in the polymer carrier PHHM, and dissociation of nanoparticles as well as further reduction of platinum (IV) prodrug into cisplatin and release of C527. Studies have shown that ID1 can promote tumor cell proliferation, inhibit cancer cell differentiation, and promote cell migration and cancer metastasis. On the one hand, C527 can inhibit the USP1 activity, which not only increases the degradation of ID1, but also reduces the ability of homologous recombination repair (HR) of cancer cells, leading to the decrease of key proteins expression in the DNA repair pathway such as FANCD2, BRCA1, and RAD51, thereby increasing the DNA damage and increasing the sensitivity of tumor cells to cisplatin. In order to investigate the ability of NP-Pt-USP1i to enhance DNA damage *in vitro*, we treated BEL-7404DPP cells with cisplatin, NP-Pt, and NP-Pt-USP1i for 48 h. Subsequently, the DNA damage related proteins were measured by Western Blot (WB). The results showed that NP-Pt-USP1i promoted the upregulation of the DNA damage markers (γ -H2AX) (Fig. 4A and B), indicating the DNA damage of tumor cells treated with NP-Pt-USP1i was significantly increased.

Next, in order to investigate the inhibition of USP1 and the degradation of ID1 by NP-Pt-USP1i, a semi-quantitative analysis of the USP1 and ID1 proteins expression was performed on the BEL-7404DPP cells treated with different drugs. The results showed that compared with NP-Pt, NP-Pt-USP1i significantly decreased the expression of USP1 and ID1 proteins (Fig. 4C and D), indicating that NP-Pt-USP1i indeed inhibited the USP1 activity of tumor cells and increased the degradation of ID1 proteins. Furthermore, the inhibitory effect of NP-Pt-USP1i on HR proteins in tumor cells was also explored. For this specific reason, BRCA1 and FANCD2 proteins were mainly selected, and the difference of their expressions in cells treated with NP-Pt-USP1i were also measured. The results showed that the expression of BRCA1 and FANCD2 proteins in cells treated with NP-Pt-USP1i was the lowest among cells treated with all drugs. Specifically, the expression of BRCA1 and FANCD2 in cells treated with NP-Pt-USP1i was 6.5 and 5.1 times lower than that of BRCA1 and FANCD2 in cells treated with NP-Pt (Fig. 4E and F), respectively. The above results indicated that NP-Pt-USP1i had a significant inhibitory effect on the ability of HR in tumor cells. Finally, to visualize the DNA damage by NP-Pt-USP1i, the γ -H2AX in cells was stained with an immunofluorescence (green) assay. We found that the green fluorescence intensity in the cell nucleus treated with NP-Pt-USP1i was significantly higher than that of cells treated with other drugs by CLSM, indicating that cells treated with NP-Pt-USP1i had significantly increased expression of γ -H2AX (Fig. 4G). To sum up, after NP-Pt-USP1i was taken up by tumor cells, cisplatin and C527 could be released through the polymer degradation, nanoparticle dissociation, and chemical reduction of the platinum (IV) prodrug to cisplatin. On the one hand, cisplatin can further cross link with DNA, causing DNA damage. On the other hand, the released C527 could further inhibit the USP1 protein activity, degrade ID1 protein, and inhibit the HR of tumor cells, thereby promoting the DNA damage, and increasing the anti-tumor effect of cisplatin.

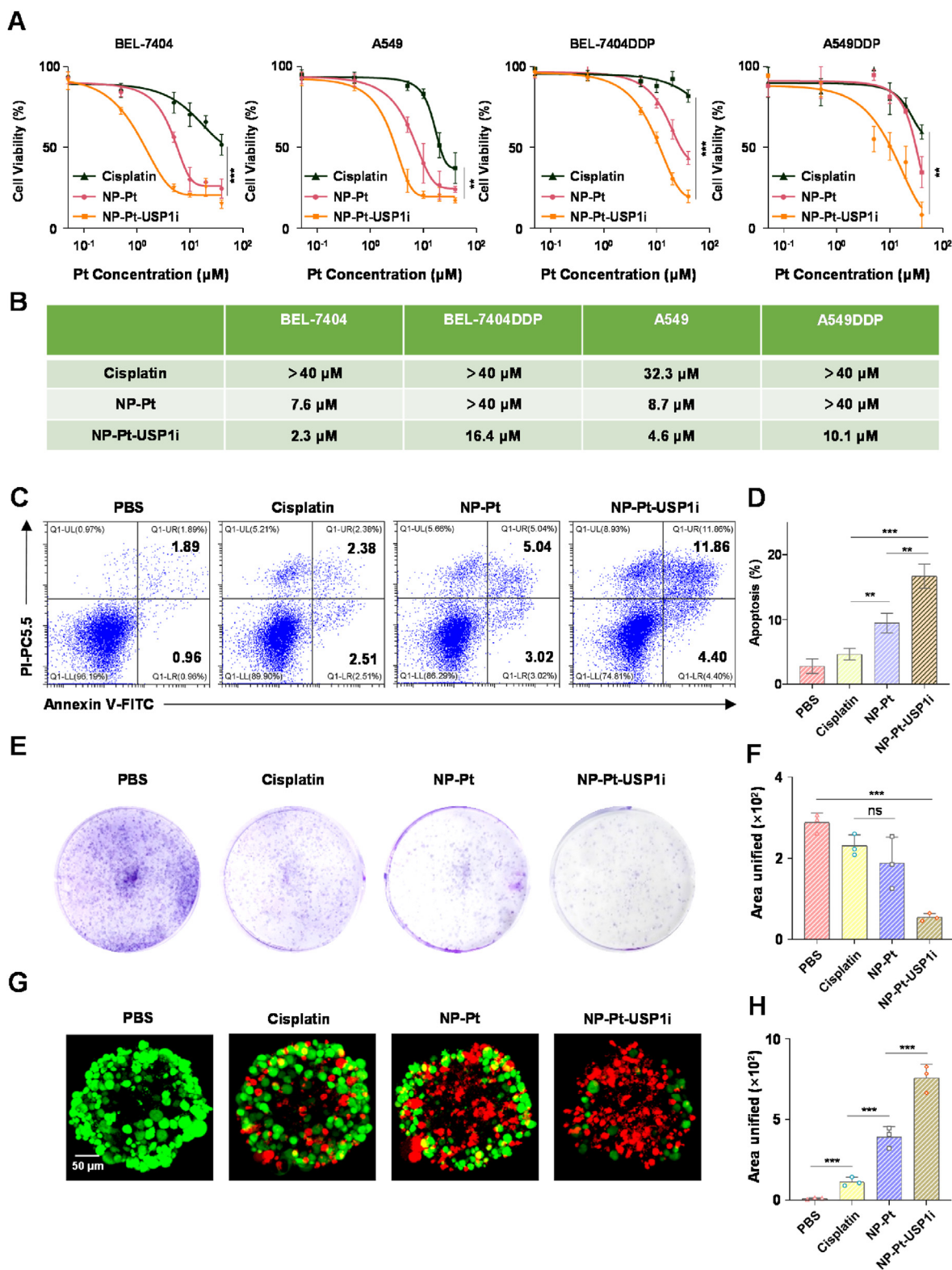
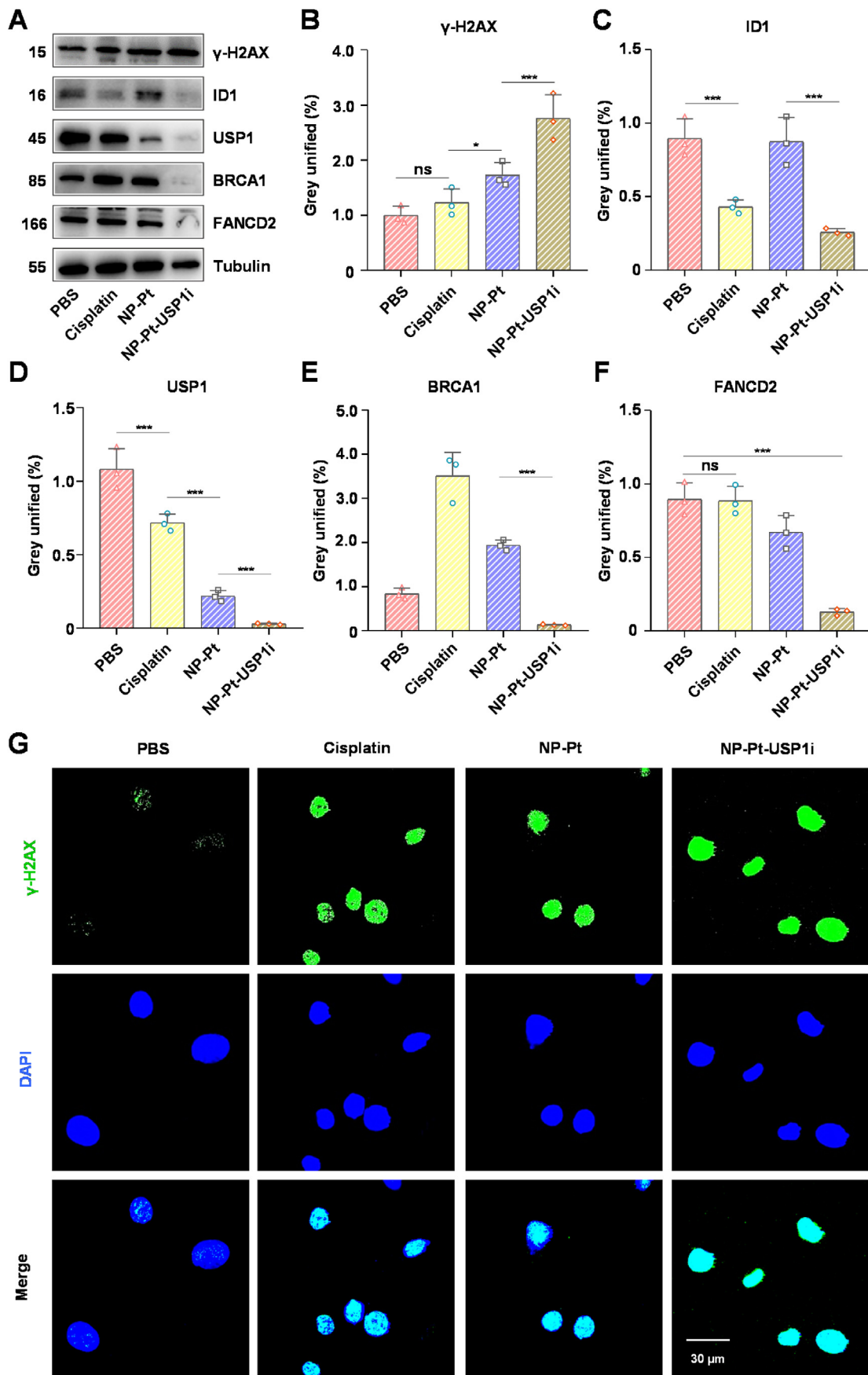


Fig. 3. *In vitro* anti-tumor effect of NP-Pt-USP1i. A) The cell survival rate of BEL-7404, BEL-7404DDP and A549, A549DDP after 48 h treatment with cisplatin, NP-Pt and NP-Pt-USP1i by an MTT assay. $^{**}p < 0.01$, $^{***}p < 0.001$ (ordinary two-way ANOVA). B) A statistical table of IC₅₀ values of BEL-7404, BEL-7404DDP and A549, A549DDP after 48 h treatment with cisplatin, NP-Pt and NP-Pt-USP1i. C) The apoptosis rate of BEL-7404DDP cells treated with different drugs by FCM. D) Semi-quantitative analysis of apoptosis rates. E) The cell colonies by a crystal violet staining assay after BEL-7404DDP cells were treated with different drugs for 10 days. F) colonies area of cells formed by Image J. G) Live and dead assay of 3D tumor spheres after 48 h treatment of PBS, cisplatin, NP-Pt and NP-Pt-USP1i. Representative CLSM images of cells stained with Calcein-AM (green, living cells) and PI (red, dead cells) were obtained. Scale bar = 50 μm . H) The statistical graphs of apoptotic cell areas by Image J of the 3D cell tumor spheres. Data are expressed in mean \pm SD from n independent experiments ($n = 3$). $^{*}p < 0.05$, $^{**}p < 0.01$, $^{***}p < 0.001$ (ordinary one-way ANOVA).



(caption on next page)

Fig. 4. NP-Pt-USP1i increased DNA damage *in vitro*. A) DNA damage protein expression. The expression of DNA damage related proteins in BEL-7404DPP cells after 48 h treatment with PBS, cisplatin, NP-Pt, and NP-Pt-USP1i was measured by Western blot. α -Tubulin is the internal reference protein. B) DNA damage related protein γ -H2AX in BEL-7404DPP cells after 48 h treatment with different drugs by Western blot. C) ID1 expression in BEL-7404DPP cells after 48 h treatment with different drugs by Western blot. D) USP1 protein expression in BEL-7404DPP cells after 48 h treatment with different drugs by Western blot. E) BRCA1 protein expression in BEL-7404DPP cells treated with different drugs for 48 h by WB. F) FANCD2 protein expression in BEL-7404DPP cells after 48 h treatment with different drugs by Western blot. G) CLSM images of DNA damage related protein γ -H2AX expression (blue, DAPI; Green, γ -H2AX). Scale bar = 50 μ m. Data are expressed in mean \pm SD from *n* independent experiments (*n* = 3). **p* < 0.05, ***p* < 0.01, ****p* < 0.001 (ordinary one-way ANOVA).

2.7. Antitumor activity of NP-Pt-USP1i *in vivo*

After verifying the anti-tumor activity and DNA damage of NP-Pt-USP1i *in vitro*, an abdominal nude mouse tumor model based on BEL-7404DPP-LUC cells was constructed for studying the anti-tumor activity of NP-Pt-USP1i *in vivo*. BEL-7404DPP-LUC cells (3×10^6 cells/mouse) were inoculated into the abdominal cavity of mice. Subsequently, the mice were treated with intraperitoneal injection of drugs for three consecutive times according to the administration schedules in Fig. 5A. The dosage of cisplatin, NP-Pt, and NP-Pt-USP1i was set at 3.5 mg Pt/kg. From the beginning day of treatment, an *in vivo* imaging system (IVIS) was used for *in vivo* imaging of the nude mice to track the changes in tumor growth in the nude mice. The change in the fluorescence intensity of the tumors at day 0, 5, 10, and 15 was recorded, respectively. At day 15, all the mice were killed, and the tumors in their abdominal cavity were taken out. Further, the tumor tissues were analyzed with hematoxylin and eosin (H&E) staining and terminal deoxynucleotidyl transfer mediated dUTP biotin nick and labeling (TUNEL) assay [29–31]. The IVIS imaging images of nude mice were shown in Fig. 5B. The results showed that the bioluminescence intensity of the nude mice treated with NP-Pt-USP1i gradually decreased with days post injection, and the average bioluminescence value after 15 days of treatment changed from the initial 9.72×10^9 p/s/cm²/sr to 1.34×10^9 p/s/cm²/sr, which was 1/50 of that of mice treated with PBS (5.74×10^{10} p/s/cm²/sr), and 1/20 of that of mice treated with NP-Pt (2.96×10^{10} p/s/cm²/sr) (Fig. 5C). The above results indicated that NP-Pt-USP1i had the highest anti-tumor effect *in vivo*. Moreover, the weight of nude mice treated with different drugs changed, there was no statistically significant difference in the weight of mice, indicating these three drugs had modest toxicity and adverse effects (Fig. 5D), and the survival rate of mice treated with NP-Pt-USP1i was considerably prolonged (Fig. 5E). Next, the therapeutic effect of NP-Pt-USP1i was further explored through H&E staining and Tunnel assay. The results showed that the necrosis area, inflammatory cell infiltration and green bioluminescence intensity of tumor tissues of mice treated with NP-Pt-USP1i were significantly higher than those of mice treated with other drugs, which fully demonstrated that NP-Pt-USP1i showed effective anti-tumor activity *in vivo* (Fig. 5F). The above results may be attributed to C527 and cisplatin released from the NPs, thereby sensitizing DNA damage, and enhancing the anti-tumor efficacy *in vivo*.

2.8. Anti-tumor activity of NP-Pt-USP1i on a PDX model

In order to further study the anti-tumor effect of NP-Pt-USP1i *in vivo*, a patient-derived xenograft (PDX) model of liver cancer was subsequently constructed. The PDX model can better stand for the pathological characteristics of tumor in clinical patients, and the drug efficacy screen results on PDX models can better represent the clinic reality, hence with greater clinic translational significance [32]. Subsequently, the anti-tumor effect of NP-Pt and NP-Pt-USP1i was evaluated on the PDX model according to a drug administration schedule (Fig. 6A). The results showed that the average tumor volumes of nude mice treated with cisplatin, NP-Pt, and NP-Pt-USP1i were 683.2 mm³, 215.6 mm³ and 92.4 mm³, respectively, and the tumor volumes of nude mice treated with NP-Pt-USP1i were equivalent to 1/2 of that of mice treated with NP-Pt (Fig. 6B). Moreover, the body weight of mice treated with NP-Pt-USP1i

did not change significantly (Fig. 6C). In addition, 18 days later, the nude mice were sacrificed and the tumors in the mice were taken out and weighed. The results showed that the average tumor weights of nude mice treated with cisplatin, NP-Pt and NP-Pt-USP1i were 1.09 g, 0.41 g and 0.13 g, respectively. The above results showed that the tumor weight of mice treated with NP-Pt-USP1i was only 1/3 of that of mice treated with NP-Pt, and the tumor weight of mice treated with NP-Pt-USP1i was compared with that of mice treated with cisplatin, and the former is only 1/8 of the latter (Fig. 6D and E). The above results once again showed that the antitumor effect of NP-Pt-USP1i was significantly higher than that of cisplatin and NP-Pt. Finally, the therapeutic effect of NP-Pt-USP1i was further verified by H&E and TUNEL staining. Through H&E staining, the nuclear fragmentation and nucleolysis of tumor cells in nude mice treated with NP-Pt-USP1i was found to be far greater than that in nude mice treated with other drugs (Fig. 6F). In addition, the results by TUNEL staining also showed that the green fluorescence intensity (DNA damage area) in tumor tissues of nude mice treated with NP-Pt-USP1i was significantly higher than that of nude mice treated with both NP-Pt and cisplatin (Fig. 6F). In conclusion, compared with cisplatin and NP-Pt, NP-Pt-USP1i displayed stronger anti-tumor effect *in vivo*.

3. Conclusion

Protein ubiquitination is the specific modification of some proteins after translation, which plays an essential role in regulating cell function and activity. Ubiquitin-specific protease 1 (USP1) is one of the most classical DUB proteins. Studies have indicated that USP1 played an important role in DNA damage responses. Fanconi anemia (FA) and DNA translesion synthesis (TLS) pathway was the first DNA damage tolerance and repair pathway found to be regulated by reversible ubiquitination. USP1 regulates DNA damage responses by de-ubiquitination of certain proteins in FA and TLS pathways, leading to drug resistance, cancer recurrence, and metastasis. Platinum anticancer drugs, such as cisplatin, oxaliplatin, and carboplatin, are the first-line anticancer alkylating agents in clinic practice. These drugs can cause DNA damage and induce cell apoptosis by cross-linking with DNAs in cancer cells. Unfortunately, the DNA repair machinery is powerful in cancer cells, resulting in drug resistance. Furthermore, DNA damage response pathways, particularly TLS and ICL repair, may have contributed to this resistance. Therefore, inhibition of DNA damage response pathways (TLS and FA) by targeting USP1 improves the sensitivity of tumor cells to cisplatin.

Here, the influence of USP1 on DNA damage response pathway in patients with liver cancer was first explored by bioinformatics analysis. We found that the expression of USP1 was positively correlated with the expression of FANCD2 and BRCA1 (Fig. 1D), and the correlation coefficients were *R* = 0.63 and *R* = 0.72, respectively. The above bioinformatics analysis showed that the expression of USP1 could promote the expression of homologous recombination repair related genes (FANCD2 and BRCA1), which negatively correlates with clinical outcome in patients with hepatocellular carcinoma. These results suggest that inhibition of the expression of USP1 has great potential to inhibit DNA repair, leading to increased DNA damage originated from DNA alkylating agents such as cisplatin, and ultimately enhancing the anti-tumor effect.

Subsequently, we verified that a selective USP1i of C527 in combination of cisplatin showed obvious synergistic anti-tumor effect, which holds great promise for further combination therapy. In this work, a

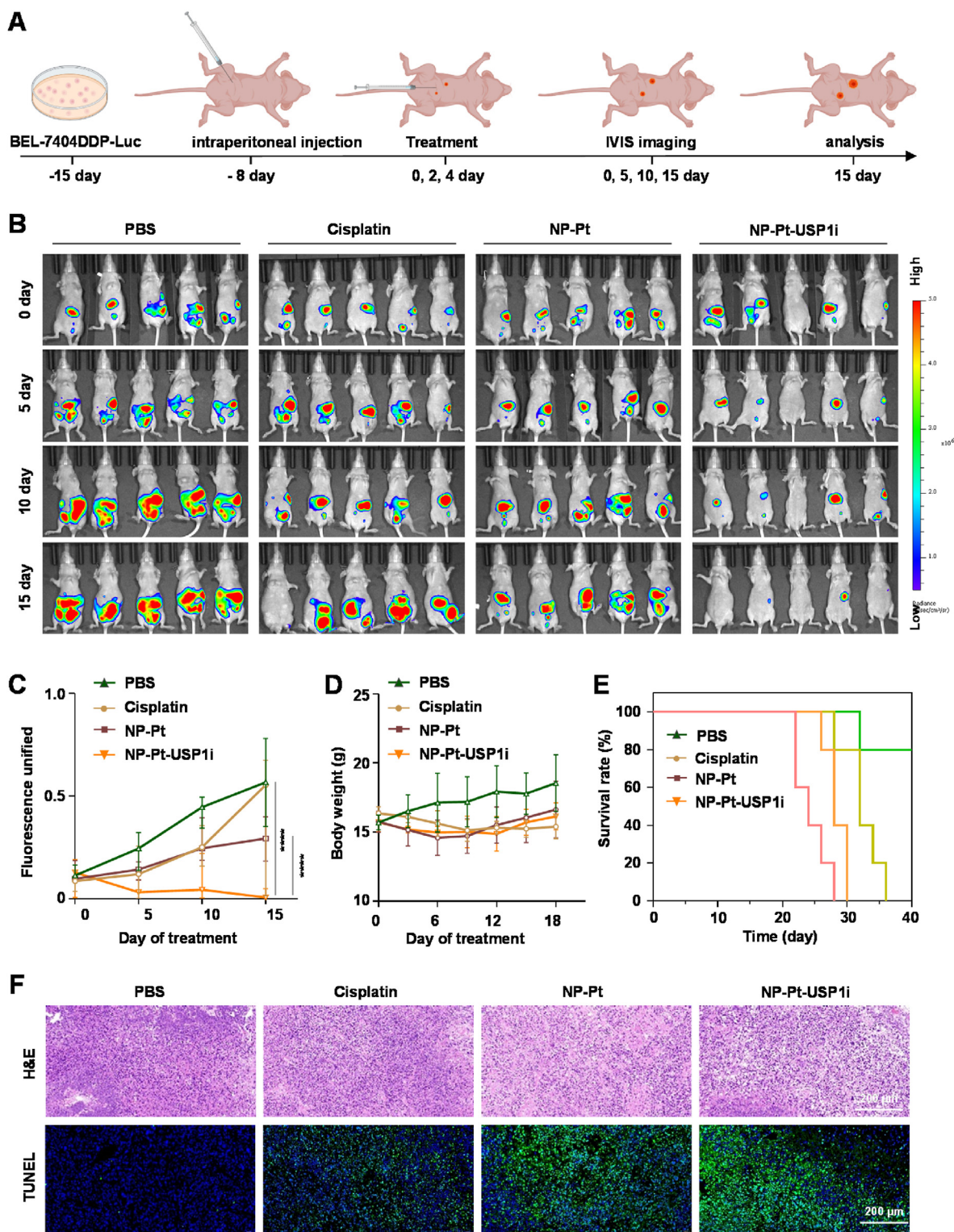


Fig. 5. The anti-tumor activity of NP-Pt-USP1i on a cisplatin resistant liver cancer model based on BEL-7404DDP/LUC cells. A) The establishment of a cisplatin resistant liver cancer mice model, and the schedule of drug administration for the anti-tumor efficacy study of NP-Pt-USP1i *in vivo*. B) The anti-tumor effect of NP-Pt-USP1i by IVIS imaging. After the nude mice with intraperitoneal tumors were treated with different drugs, they were imaged *in vivo* with IVIS at 0, 5, 10 and 15 days respectively. C) The anti-tumor effect of NP-Pt-USP1i *via* semi-quantitative analysis of bioluminescence intensity, *** $p < 0.001$ (ordinary two-way ANOVA). D) The changes in body weight of mice treated with NP-Pt-USP1i. E) Survival of mice with different treatments. F) After 15 days of drug treatment, representative H&E and TUNEL staining of tumors treated with various drugs were obtained. Scale bar = 200 μm . Data are expressed in mean \pm SD from n independent experiments ($n = 5$).

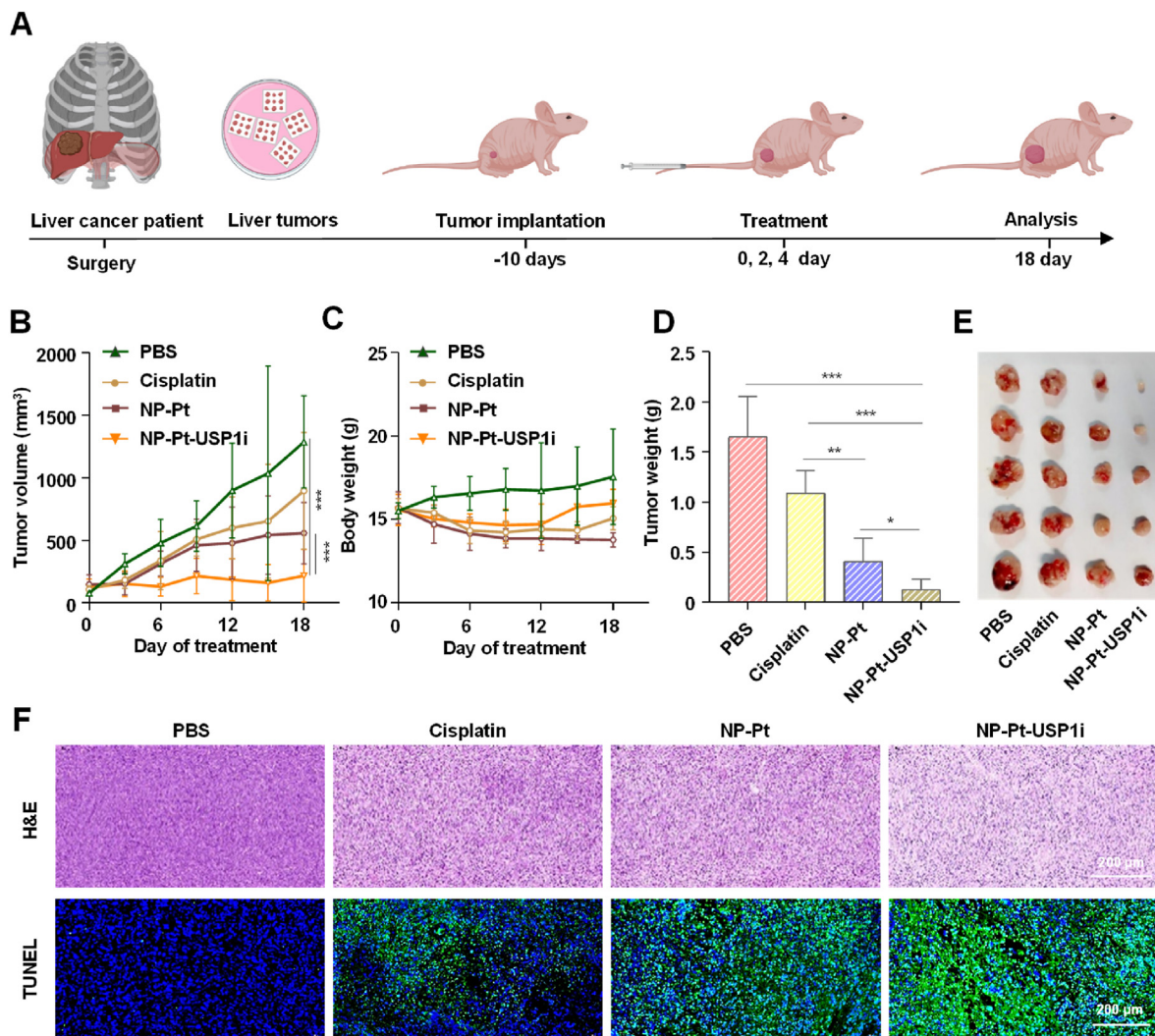


Fig. 6. NP-Pt-USP1i showed strong anti-tumor activity on a PDX mice model. A) The establishment of a PDX model of liver cancer on nude mice and the schematic schedule of drug administration. B) Tumor growth inhibition curves of nude mice bearing PDX tumors treated with different drugs, $***p < 0.001$ (ordinary two-way ANOVA). C) Quantitative analysis of tumor weights of tumors of PDX nude mice treated with different drugs after 18 days. D) Body weight change curve of nude mice bearing PDX tumors treated with different drugs after 18 days. E) Photos of tumors of nude mice bearing PDX tumors treated with different drugs after 18 days. F) H&E and TUNEL staining of representative tumors in nude mice bearing PDX tumors after 18 days of drug treatment. Data are expressed in mean \pm SD from n independent experiments ($n = 5$). * $p < 0.05$, ** $p < 0.01$, *** $p < 0.001$ (ordinary one-way ANOVA).

disulfide bonded polymer carrier was designed and adopted to encapsulate a USP1i and a platinum (IV) prodrug to form NP-Pt-USP1i. NP-Pt-USP1i was able to effectively inhibit tumor progression on a cell-line derived cancer model of BEL-7404DPP cell lines as well as a PDX model of liver cancer. In conclusion, the use of USP1i combined with a platinum (IV) prodrug in nanoparticles could inhibit the growth of liver cancer. The results shown in this paper demonstrate a future precise cancer therapy with DNA damaging agents of cisplatin with USP1i to overcome cisplatin resistance in clinic.

Credit author statement

Kun Shang: Data curation, Writing – original draft. Lingpu Zhang: Conceptualization, Methodology. Yingjie Yu: Writing- Reviewing and Editing. Haihua Xiao: Writing- Reviewing and Editing. Yajuan Gao: Data curation. Liu Yang: Data curation. Jia Huang: Supervision, Funding acquisition. Haiqin Song: Writing-Reviewing and Editing, Supervision, Funding acquisition. Hongbin Han: Writing- Reviewing and Editing, Funding acquisition, Project administration.

Declaration of competing interest

The authors declare that they have no known competing financial interests or personal relationships that could have appeared to influence the work reported in this paper.

Data availability

Data will be made available on request.

Acknowledgements

This work was supported by National Natural Science Foundation of China (NO: 51803120); Jiangsu Specially-Appointed Professor Talent Program and Guangci Distinguished Young Scholars Training Program of Ruijin Hospital (NO: GCQN-2019-A06); Tianyuan of National Natural Science Foundation of China (12126601); Shenzhen Science and Technology Program (NO: KQTD20180412181221912); Project of Beijing's advanced and sophisticated discipline (BMU2019GJJXK006).

Appendix A. Supplementary data

Supplementary data to this article can be found online at <https://doi.org/10.1016/j.mtbio.2023.100548>.

References

- [1] M. Rape, *Nat. Rev. Mol. Cell Biol.* 19 (2018) 59–70.
- [2] M. Scheffner, U. Nuber, J.M. Huibregtse, *Nature* 373 (1995) 81–83.
- [3] D. Komander, *Biochem. Soc. Trans.* 37 (2009) 937–953.
- [4] Y. Li, Y. Xu, C. Gao, Y. Sun, K. Zhou, P. Wang, J. Cheng, W. Guo, C. Ya, J. Fan, X. Yang, *Front. Oncol.* 10 (2020), 554809.
- [5] F. Geng, S. Wenzel, W.P. Tansey, *Annu. Rev. Biochem.* 81 (2012) 177–201.
- [6] F. Bassermann, R. Eichner, M. Pagano, *Biochim. Biophys. Acta* 1843 (2014) 150–162.
- [7] D. Vucic, V.M. Dixit, I.E. Wertz, *Nat. Rev. Mol. Cell Biol.* 12 (2011) 439–452.
- [8] V.H. Oestergaard, F. Langevin, H.J. Kuiken, P. Pace, W. Niedzwiedz, L.J. Simpson, M. Ohzeki, M. Takata, J.E. Sale, K.J. Patel, *Mol. Cell* 28 (2007) 798–809.
- [9] S. Lipkowitz, A.M. Weissman, *Nat. Rev. Cancer* 11 (2011) 629–643.
- [10] I. Garcia-Santisteban, G.J. Peters, E. Giovannetti, J.A. Rodriguez, *Mol. Cancer* 12 (2013) 91.
- [11] D. Komander, M. Rape, *Annu. Rev. Biochem.* 81 (2012) 203–229.
- [12] H.C. Tai, E.M. Schuman, *Nat. Rev. Neurosci.* 9 (2008) 826–838.
- [13] A.M. Weissman, N. Shabek, A. Ciechanover, *Nat. Rev. Mol. Cell Biol.* 12 (2011) 605–620.
- [14] M. Sonogo, I. Pellarin, A. Costa, G.L.R. Vinciguerra, M. Coan, A. Kraut, S. D'Andrea, A. Dall'Acqua, D.C. Castillo-Tong, D. Califano, S. Losito, R. Spizzo, Y. Coute, A. Vecchione, B. Belletti, M. Schiappacassi, G. Baldassarre, *Sci. Adv.* 5 (2019) eaav3235.
- [15] K.S. Lim, H. Li, E.A. Roberts, E.F. Gaudiano, C. Clairmont, L.A. Sambel, K. Ponninselvam, J.C. Liu, C. Yang, D. Kozono, K. Parmar, T. Yusufzai, N. Zheng, A.D. D'Andrea, *Mol. Cell* 72 (2018) 925–941 e924.
- [16] S.M. Nijman, T.T. Huang, A.M. Dirac, T.R. Brummelkamp, R.M. Kerkhoven, A.D. D'Andrea, R. Bernards, *Mol. Cell* 17 (2005) 331–339.
- [17] A. Ma, M. Tang, L. Zhang, B. Wang, Z. Yang, Y. Liu, G. Xu, L. Wu, T. Jing, X. Xu, S. Yang, Y. Liu, *Oncogene* 41 (2022) 1673.
- [18] S.A. Williams, H.L. Maecker, D.M. French, J. Liu, A. Gregg, L.B. Silverstein, T.C. Cao, R.A. Carano, V.M. Dixit, *Cell* 146 (2011) 918–930.
- [19] Q. Liang, T.S. Dexheimer, P. Zhang, A.S. Rosenthal, M.A. Villamil, C. You, Q. Zhang, J. Chen, C.A. Ott, H. Sun, D.K. Luci, B. Yuan, A. Simeonov, A. Jadhav, H. Xiao, Y. Wang, D.J. Maloney, Z. Zhuang, *Nat. Chem. Biol.* 10 (2014) 298–304.
- [20] D.A. Fennell, Y. Summers, J. Cadranel, T. Benepal, D.C. Christoph, R. Lal, M. Das, F. Maxwell, C. Visseren-Grul, D. Ferry, *Cancer Treat Rev.* 44 (2016) 42–50.
- [21] H.H. Xiao, L.S. Yan, E.M. Dempsey, W.T. Song, R.G. Qi, W.L. Li, Y.B. Huang, X.B. Jing, D.F. Zhou, J.X. Ding, X.S. Chen, *Prog. Polym. Sci.* 87 (2018) 70–106.
- [22] L. Zhang, K. Shang, X. Li, M. Shen, S. Lu, D. Tang, H. Han, Y. Yu, *Adv. Funct. Mater.* 32 (2022), 2204589.
- [23] L. Zhang, Y. Wang, J. Karges, D. Tang, H. Zhang, K. Zou, J. Song, H. Xiao, *Adv. Mater.* (2022), e2210267.
- [24] Y. Wang, Y. Jiang, D. Wei, P. Singh, Y. Yu, T. Lee, L. Zhang, H.K. Mandl, A.S. Piotrowski-Daspit, X. Chen, F. Li, X. Li, Y. Cheng, A. Josowitz, F. Yang, Y. Zhao, F. Wang, Z. Zhao, A. Huttner, R.S. Bindra, H. Xiao, W. Mark Saltzman, *Nat. Biomed. Eng.* 5 (2021) 1048–1058.
- [25] D. Wei, Y. Yu, X. Zhang, Y. Wang, H. Chen, Y. Zhao, F. Wang, G. Rong, W. Wang, X. Kang, J. Cai, Z. Wang, J.Y. Yin, M. Hanif, Y. Sun, G. Zha, L. Li, G. Nie, H. Xiao, *ACS Nano* 14 (2020) 16984–16996.
- [26] J. Chen, X. Wang, Y. Yuan, H. Chen, L. Zhang, H. Xiao, J. Chen, Y. Zhao, J. Chang, W. Guo, X.J. Liang, *Sci. Adv.* 7 (2021).
- [27] D. Wei, Y. Huang, B. Wang, L. Ma, J. Karges, H. Xiao, *Angew Chem. Int. Ed. Engl.* 61 (2022), e202201486.
- [28] M. Ravera, E. Gabano, M.J. McGlinchey, D. Osella, *Dalton Trans.* 51 (2022) 2121–2134.
- [29] L. Zhang, L. Zhu, L. Tang, J. Xie, Y. Gao, C. Yu, K. Shang, H. Han, C. Liu, Y. Lu, *Adv. Sci.* (2022), e2205246.
- [30] G. Xiong, D. Huang, L. Lu, X. Luo, Y. Wang, S. Liu, M. Chen, S. Yu, M. Kappen, C. You, S. Lu, Y. Yu, J. Lu, F. Lin, *Small Methods* 6 (2022) 2200379.
- [31] Y. Yu, L. Zhang, Z. Qin, J. Karges, H. Xiao, X. Su, *Adv. Funct. Mater.* 33 (2023) 2208797.
- [32] W. Wang, J. Cai, J. Wen, X. Li, Y. Yu, L. Zhang, Q. Han, W. Zheng, Y. Ma, F. Ying, X. Xu, W. Li, Q. Yang, S. Sun, X. He, L. Cai, H. Xiao, Z. Wang, *Nano Today* 44 (2022) 101459.